Metal–Organic Frameworks

DOI: 10.1002/anie.200804739

Crystallographic Observation of Dynamic Gas Adsorption Sites and Thermal Expansion in a Breathable Fluorous Metal–Organic Framework**

*Chi Yang, Xiaoping Wang, and Mohammad A. Omary**

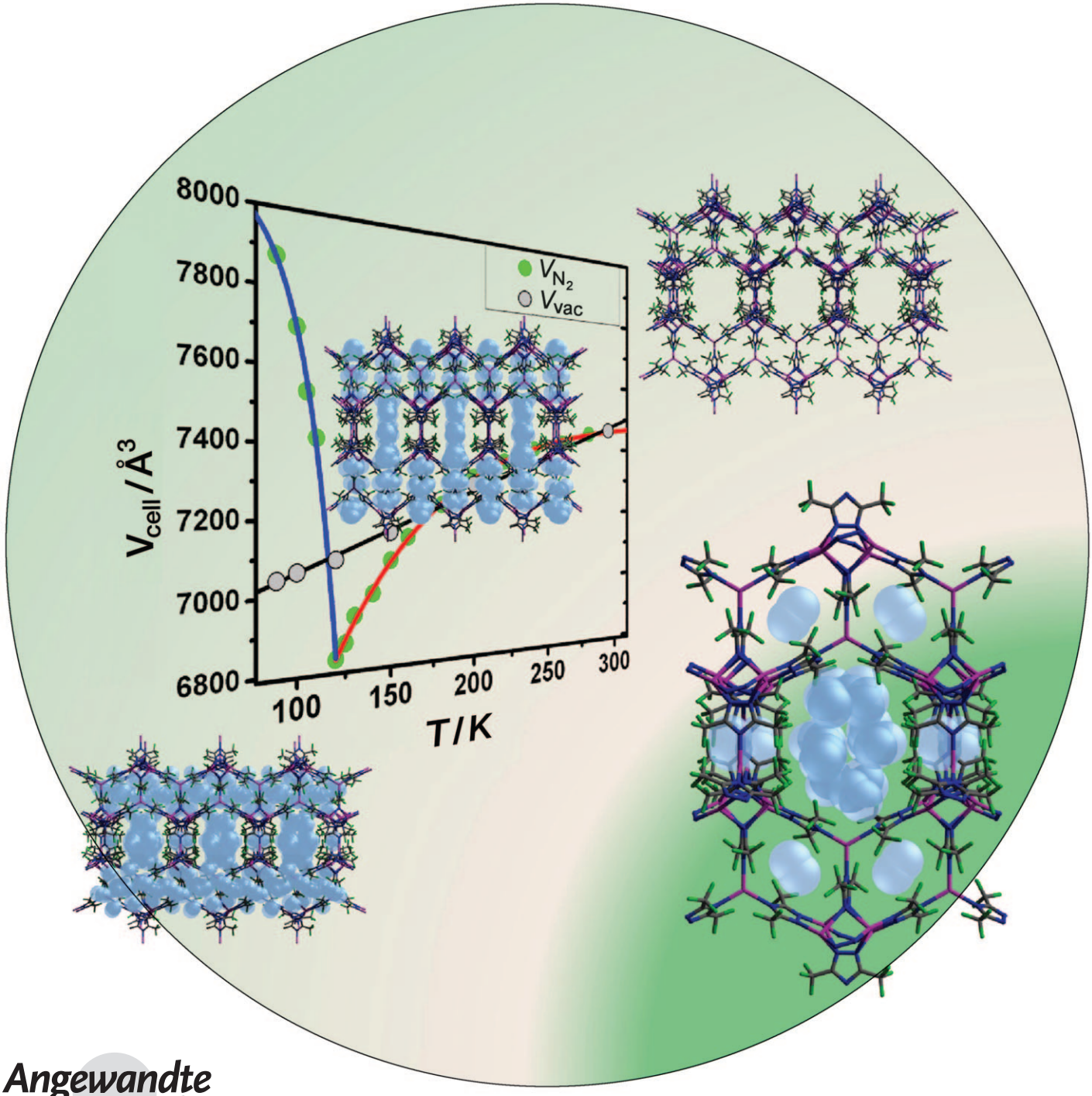

Crystal breathing upon gas adsorption is an unusual phenomenon with potential break-through impacts on gas storage, exchange, and transport by metal–organic frameworks (MOFs).[1–3] Férey and co-workers have demonstrated that some flexible MOFs exhibit remarkable volume expansions upon liquid uptake.[4,5] Precise determination of gas adsorption sites is of paramount importance for new research efforts toward MOFs with improved gas storage capacity or separation ability. While such studies have been reported for a few rigid MOFs,[6–8] there is only one precedent for the location of gas adsorption sites in a flexible MOF; this study was carried out using synchrotron powder diffraction at an intermediate adsorption stage.[9] The search for breathable single crystals remains a challenge, as such crystals usually do not survive large volume expansions. Fluorous metal–organic frameworks (FMOFs)[10] are new porous materials that show enhanced thermal, light, and air stability; superacidity; and low surface energy and surface tension in addition to other excellent optical and electrical properties known for fluorous materials.[11–13] We have recently communicated the high-density gas uptake and unique hysteretic sorption of H_2 within FMOF-1, the first example in the FMOF family, which we derived from silver(I) and 3,5-bis(trifluoromethyl)-1,2,4-triazolate (Tz).[10] Herein we show that FMOF-1 undergoes remarkable breathing and thermal expansion with very large changes in volume and unit-cell parameters upon cooling single crystals in the presence or absence of gas molecules. This work also describes the dynamic gas adsorption mechanism at the atomic level to illustrate the sequential filling of the multiple gas adsorption sites in both small and large pores within FMOF-1 and the consequent remarkable swelling of these framework cavities.

We utilized single crystal X-ray diffraction to determine the temperature dependence (295→90 K) of the structures of two evacuated single crystals of FMOF-1; one crystal was directly exposed to a constant N_2 stream at ambient pressure from the cryostream of the diffractometer, while the other was cooled in a vacuum-sealed (10^{-3} Torr) glass capillary. All structures for both crystals maintained a tetragonal structure (space group $I\bar{4}2d$)[10] at all temperatures investigated. The variation of the unit-cell parameters with temperature is illustrated in Figure 1. For the crystal exposed to N_2 atmosphere, the crystallographic data indicate remarkable two-step breathing. First, the crystal smoothly contracts on cooling from a volume of 7461.8(6) Å^3 at 295 K to 6823.7(4) Å^3 at 119 K, an 8.6% decrease following an exponential decay, $V = 7501 - 685 \times \exp[(119-T)/64]$ (Figure 1a, red line). Second, the sign of the apparent thermal expansion changes as the crystal exponentially expands to a volume of 7719.1(3) Å^3 on further cooling towards 90 K, a dramatic increase of 13.1% following $V = 8094 - 1192 \times \exp[(T-119)/17]$ (Figure 1a, blue line). The apparent thermal expansion behavior in the crystal under N_2 is anisotropic (Figure 1b,c). While the unit-cell parameters a and b show a trend parallel to the cell volume V, the parameter c shows an opposite trend. On cooling from 295 to 119 K, a and b shrink from 14.0733(5) to 12.950(4) Å, while c expands from 37.675(3) to 40.69(2) Å; on further cooling from 119 to 90 K, a and b drastically increase to 14.726(2) Å, while c rapidly decreases to 35.59(1) Å.

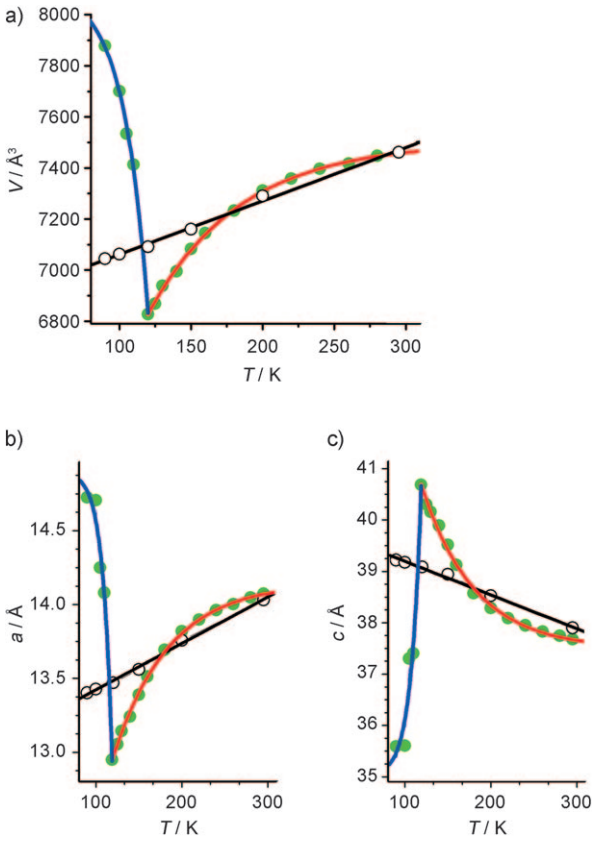

Figure 1. Temperature evolution of structural parameters of FMOF-1 under a constant stream of N_2 at ambient pressure (●) and under vacuum (○): a) Unit-cell volume V. b) Lattice constant $a = b$. c) Lattice constant c. The red and blue lines are first-order exponential decay fitting curves of PTE (295→119 K) and NTE (119→90 K) under N_2, respectively. The black lines represent the linear fitting of the unit-cell parameters for the crystal in vacuum: $V = 6852.3 + 2.09\,T$; $a = 13.107 + 0.00315\,T$; $c = 39.8536 - 0.00657\,T$.

In contrast to the behavior of the crystal exposed to N_2, the vacuum-sealed crystal shows linear thermal expansion with a rate of $(\partial V/\partial T)_p = +2.09$ Å^{3}K^{-1} that describes linear thermal contraction upon cooling in the entire 295→90 K range (Figure 1, black circles). This behavior clearly indicates that the anomalous expansion of the FMOF-1 crystal under N_2 upon cooling is correlated to the location of N_2 gas molecules in the framework voids (see below). The thermal expansion within the FMOF-1 crystal under vacuum is also

[*] Dr. C. Yang, Dr. X. Wang,[+] Prof. Dr. M. A. Omary
Department of Chemistry, University of North Texas
Denton, TX 76203 (USA)
E-mail: omary@unt.edu
[+] Current address: Oak Ridge National Laboratory
One Bethel Valley Road, PO Box 2008 MS6460
Oak Ridge TN 37831 (USA)
[**] This work resulted from research support by the U. S. National Science Foundation (CHE-0349313), the Robert A. Welch Foundation (B-1542), the Texas Advanced Research Program (009741-0089-2007), and the U. S. Department of Energy (DE-FC26-06NT42859).
Supporting information for this article is available on the WWW under http://dx.doi.org/10.1002/anie.200804739.

anisotropic (Figure 1b,c). Upon cooling from 295 to 90 K, the unit-cell parameters a and b shrink with a rate of $(\partial a/\partial T)_p = (\partial b/\partial T)_p = +3.15\times10^{-3}$ Å K^{-1}, a uniaxial positive thermal expansion (PTE), whereas the parameter c expands with a rate of $(\partial c/\partial T)_p = -6.57\times10^{-3}$ Å K^{-1}, a uniaxial negative thermal expansion (NTE). The volumetric thermal expansion coefficient $\beta = (1/V)(\partial V/\partial T)_p$ and the linear thermal expansion coefficients $\alpha_a = (1/a)(\partial a/\partial T)_p$ and $\alpha_c = (1/c)(\partial c/\partial T)_p$ for FMOF-1 under vacuum are $\beta = +3.0\times10^{-4}$ K^{-1}, $\alpha_a = +2.3\times10^{-4}$ K^{-1}, and $\alpha_c = -1.7\times10^{-4}$ K^{-1}, which are higher than the coefficients characterizing the thermal expansion behavior deemed "colossal" for $Ag_3[Co(CN)_6]$ ($\beta = +1.6\times10^{-4}$ K^{-1}, $\alpha_a = +1.5\times10^{-4}$ K^{-1}, $\alpha_c = -1.3\times10^{-4}$ K^{-1}), as reported very recently by Goodwen et al.[14]

In contrast to the pure thermal expansion by the crystal under vacuum, the apparent NTE behavior of FMOF-1 under N_2 atmosphere is a new phenomenon for single crystal breathing that occurs upon gas adsorption.[9] Although the NTE terminology has been invoked in the literature for MOFs that likewise include guest molecules at low temperatures (e.g., 1.2% volume increase for N_2-loaded MOF-5 upon cooling from 293 to 30 K),[6] we qualify this situation as "apparent" to distinguish it from the pure thermal expansion in the absence of guest molecules. Nevertheless, a comparison can be made to demonstrate the huge apparent NTE and PTE rates exhibited by single crystals of FMOF-1 under N_2 at ambient pressure. The thermal expansion coefficients for the overall NTE process in the 119→90 K range for FMOF-1 under N_2 achieve $\beta = -1.0\times10^{-2}$ K^{-1}, $\alpha_a = -1.3\times10^{-2}$ K^{-1}, and $\alpha_c = 1.2\times10^{-2}$ K^{-1}, which are three orders of magnitude higher than the prototypical NTE material ZrW_2O_8[15] and more than two orders of magnitude greater than the recent simulated values for the isoreticular IRMOFs ($\alpha \leqq -2.7\times10^{-5}$ K^{-1}).[16,17] The analogous thermal expansion coefficients for the overall PTE process in the 295→119 K range are $\beta = 1.3\times10^{-3}$ K^{-1}, $\alpha_a = 1.4\times10^{-3}$ K^{-1}, and $\alpha_c = -1.3\times10^{-3}$ K^{-1}, which are significantly greater than the corresponding values for the crystal in vacuum (see above) and represent nearly an order of magnitude increase over those for $Ag_3[Co(CN)_6]$.[14]

What are the structural characteristics of the framework that impart the flexibility to allow such a drastic, reversible, and anisotropic expansion? The structure of FMOF-1 consists of $[Ag_4Tz_6]$ clusters that interconnect through three-coordinate Ag^I atoms, giving rise to two types of voids: interconnected microporous tunnels along both the a and b axes and toroid-shaped nanocages within the walls surrounding the channels (Figure 2). The tunnel consists of an infinitely connected embedded fluorine-lined minimal surface that is triply periodic with triple junctions. The cages can be topologically represented as toroids, the larger and smaller openings of which are exposed to two adjacent channels. The defining features of the cages are their two portals, each of which consists of two pairs of flexible CF_3 rotors that provide entry to their hydrophobic cavity. Unlike typical molecular containers (e.g., cyclodextrins),[18] the depth, equatorial width, annular width, and volume of the cage vary dramatically with temperature. As seen in Figure 2, the Tz ligands and Ag_4 cores do not exhibit significant changes during the

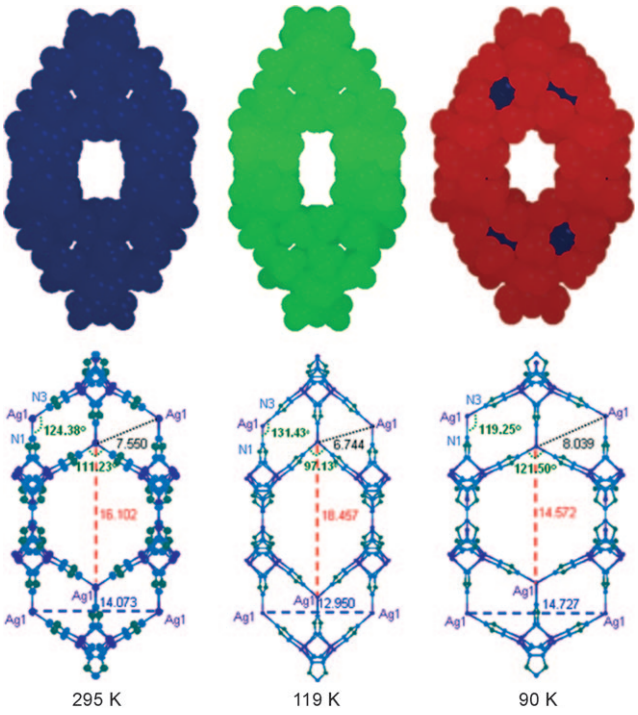

Figure 2. Top: Space-filling representations showing the size and shape evolution of the channel and toroid cage of FMOF-1 during the first (295→119 K) and second (119→90 K) breathing steps. Bottom: ORTEP plots showing perspective views of the correlative evolution of the CF_3-free framework skeleton seen along [100].

two breathing processes. The most drastic change results from the coordination geometry around the three-coordinate Ag1 linker that interconnects the $[Ag_4Tz_6]$ units into 3D frameworks. The Ag1 linker sits at the crossroad of three Tz ring planes; the Ag1–N3 bond length remains essentially constant from 295 K (2.297(7) Å) to 119 K (2.304(2) Å), then shrinks to 2.268(5) Å at 90 K. The Ag1–N1 bond length decreases from 2.247(10) Å at 295 K to 2.203(4) Å at 119 K, and then drastically elongates to 2.273(7) Å at 90 K. Concomitantly, the N3-Ag1-N3 angle first shrinks from 111.2(4)° at 295 K to 97.13(12)° at 119 K and then significantly expands to 121.5(2)° at 90 K. During these transformations, the Tz rings and CF_3 groups change their respective angular orientations to accommodate the constraints and minimize the lattice energy. This "mechanical" process, allowed by both the directivity of the linker covalent bonds and the flexibility of the Ag^I–N coordination bonds, explains the dynamic transformations induced by the host–guest interactions within FMOF-1.

The change in bond lengths and angles results in a large anisotropic unit-cell expansion that is reflected in the size and shape changes of the channels and cages within FMOF-1 (Figure 2). During the first breathing step (295→119 K), the channel narrows and changes shape from a nearly round to a nearly flat rectangle, whereas the second breathing step (119→90 K) causes the smoothed channel to broaden and curve in, giving rise to an eight-fold inward-hollowed geometry. The cage remains closed to guest molecules during the first breathing step and then opens during the

second breathing step. These changes are illustrated by considering the CF_3-free frameworks (Figure 2, bottom). Thus, the cross-window hexagon of the channel and the cross-window parallelogram of the cage both narrow and elongate (295→119 K) such that the diagonal of the hexagon (d) increases by 14.6% while the diagonal of parallelogram (d') decreases by 10.7%. The internal angle (θ) of the hexagon decreases by 13.6% while the internal angle of the parallelogram (θ') increases by 6.6%. On the other hand, the channel and cage widen and shorten during the 119→90 K breathing such that d decreases by 21.0% while d' increases by 19.2%, whereas θ increases by 25.4% while θ' decreases by 10.0%.

The consequences of these reversible and anisotropic changes for the solvent-accessible volume in FMOF-1 are rather significant. The V_{void}/V_{cell} ratio decreases from 43.6% at 295 K to 37.8% at 119 K, and then increases to 47.3% at 90 K. The contribution from the cage is 1.1% at 295 K (cage accessible, $V_{cage} = 10$ Å^3), 0% at 119 K (cage closed), and 4.1% at 90 K (cage fully open, $V_{cage} = 40$ Å^3).[19] The internal surface area[20] decreases from 901.1 $m^2 cm^{-3}$ at 295 K to 838.3 $m^2 cm^{-3}$ at 119 K and then rapidly increases to 1005.0 $m^2 cm^{-3}$ at 90 K, showing a similar temperature dependence as that of the voids.

The underlying mechanism of the breathing and anisotropic expansion within FMOF-1 can be understood by a precise determination of the evolution and occupancies of the gas adsorption sites during the thermal expansion process. X-ray crystallographic data were collected from single crystals of FMOF-1 under an N_2 stream and under vacuum between 295 and 90 K. Refinement of the data for a vacuum-sealed crystal confirmed the linear thermal expansion of the tetragonal unit cell and the absence of guest molecules in the pores over the entire 295–90 K range. In contrast, localization of N_2 molecules in voids of FMOF-1 under the nitrogen stream is apparent at 150 K and becomes significant at approximately 125 K. The localized N_2 molecules first occupy the most curvatured site close to the Ag1 linker in the channel corner, with close contacts to the two coordinating Tz rings. This site (denoted as site I), which represents the first primary adsorption site, is evident even at temperatures as high as 150 K. Occupation of this site causes channel narrowing owing to the attraction between N_2 molecules and Tz ring pairs in the corner. Refinement of data collected at 150, 125, and 119 K indicates that, upon cooling, the occupancy at site I increases from 0.30 at 150 K to 0.65 at 125 K and then to 1.0 at 119 K, causing the crystal to contract increasingly and anisotropically (Figure 2). The characteristic distances between the N_2 molecule in site I and the corner Ag1 atom, Tz centroid, and nearest CF_3 groups all continuously decrease upon cooling. The respective values at 150, 125, and 119 K are as follows: N1s···Ag1 5.77, 5.56, 5.53 Å; N1s···Centroid_Tz 4.30, 4.08, 3.90 Å; N1s···F8 3.16, 3.15, 3.18 Å. After binding at the corner site, there is a gradual occupation of site II, which lies at distances of 3.88 and 3.79 Å from four pairs of CF_3 groups of the cage portal unit (N2s···F7 3.88, N2s···F9 3.91, N2s···F2 3.79, N2s···Ag1 6.01 Å). The labyrinth windows accessing these pores are filled next, with the N_2 molecule residing at the centers of these windows 3.63 Å (N3s···F5) and 3.84 Å (N3s···F9) away from two pairs of CF_3 groups. The intersite distance is 3.30 Å between site I and site II, and 3.58 Å between site II and site III. The data between 295 and 119 K reveal that N_2 molecules are located in a flat monolayer distribution between the fluorine-lined channel surface along the a and b directions, which is consistent with the flat, smooth, and narrow shape of the channels of FMOF-1 during the first breathing process.

Further cooling below 119 K leads to enormous expansion of the channels owing to the mutual repulsion between N_2 molecules concomitant with their increased attraction to the channel walls. It is reasonable to propose that when site I is fully occupied, the N_2 molecules then closely and increasingly approach and occupy the cage portal site II, which forces the cage gate CF_3 pairs to open and allow the N_2 molecules to access the interior of the cage. To accommodate the N_2 molecules, the cages have to expand, which simultaneously induces the channels to swell. As shown in Figure 3b,c, each cage can trap one N_2 molecule (site C), and the broadened channel can accommodate more than five symmetry-independent N_2 molecules through its increased volume and surface area and its curved sites (Figure 2). The corner site I has two-fold symmetry-related locations, and there are sixteen of these sites per unit cell. The portal site II is aligned with a two-fold axis, allowing a closer approach of one atom of N_2 (N2s) to the cage gate. The labyrinth site III is also strongly associated with the $[Ag_4Tz_6]$ cluster, interacting with two separate CF_3 groups through electrostatic N···F attraction. In addition to sites I–III, which are now closer to the channel wall than they were above 119 K, analysis of the data at 90 and 100 K reveals binding of one N_2 molecule in the cage (site C) and partial occupation of two additional sites (site IV, V) during the second breathing step. The N_2 molecule at site IV lies close to the back gate of the cage, whereas the N_2 molecule at site V lies 3.45 (N5s···F5) and 3.59 Å (N5s···F9) away from the CF_3 groups at the hexagonal corner. The filling of highly curved then less-curved surface sites is consistent with the theory of micropore filling.[21] These results complement our previous low-pressure N_2 and O_2 sorption and high-pressure H_2 sorption isotherms for this material, which indicated a two-step pore-filling sequence.[10]

The cage cavity site (site C) is critical, because its filling manifests the initiation of the large breathing that causes the apparent NTE behavior of FMOF-1. Data refined at 90 K indicate that N_2 molecules located in the cage are oriented to the corner of the cage. Site C exhibits strong π interactions with a pair of Tz rings (N1c···Centroid_Tz 3.12 Å) and electrostatic attraction with the front gate CF_3 groups (N1c···F1 3.17 Å, N1c···F3 3.20 Å; Figure 3c). The front and back portals guarding the entry to the cavity of the cage are approximately 1.2 and 3.1 Å narrower than the cavity itself, which results in constrictive binding that produces significant steric barriers to guest association and dissociation. These electrostatic attractions, combined with the electron delocalization effect and the steric barriers imposed by the smaller opening of the cage, strongly confine the N_2 molecule in the cage. This gated small hollow cage, therefore, functions like a nanomachine for gas storage and exchange, a structural and functional mimic of the mammalian lung alveoli.[22]

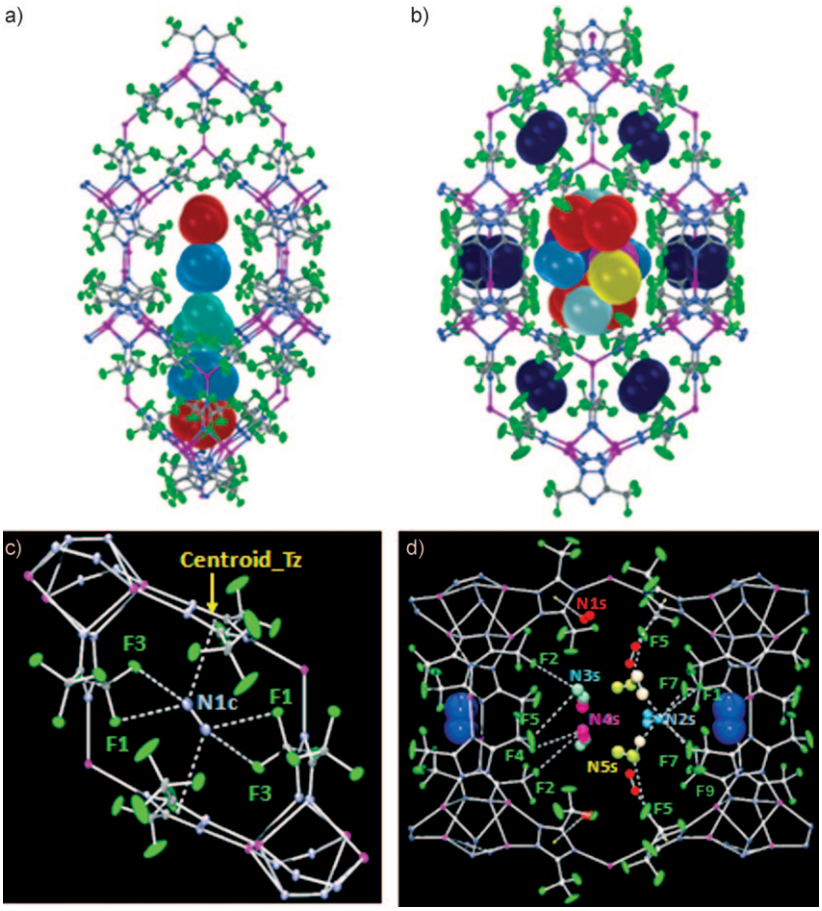

Figure 3. Gas adsorption sites in FMOF-1. a) 119 K: site I (dark red) at corner; site II (dark blue) at cage portal; site III (turquoise) at labyrinth. b) 100 K: Cage site C (light blue); channel sites I–III: same as in 119 K structure; site IV (yellow green) at the back smaller portal of cage; site V (violet) near CF_3 groups at corners. c–d) Shortest interatomic contacts of N_2 molecules at 100 K [Å]: c) Cage site C: N1c···Tz centroid 3.116; N_2···CF_3: N1c ···F1 3.171, N1c···F3 3.204. d) Channel site I: Tz centroid 3.184, 2 F3 3.220; site II: 2 F3 3.328, 2 F7 3.417; site III: F2 3.533, F1 3.342; site IV: F2 3.333, F4 3.300; site V: F9 3.592, F5 3.454.

Determination of the precise location of multiple adsorption sites in FMOF-1 grants rare insight into the dynamic framework channel and cage structures. Our findings also shed light on the mechanism for hysteretic gas adsorption in FMOF-1.[10] The two-step loading found for the adsorption of N_2, O_2, and H_2 into FMOF-1 can be related to the apparent PTE and NTE processes, whereas the hysteretic one-step gas desorption implies that the delayed gas desorption from the cage occurs after gas desorption from the channel. It is likely that the crystal contraction induced by the channel gas desorption results in concomitant release of gas molecules in the cage.

In summary, we have characterized the breathing motion within FMOF-1 in three ways: 1) the breathing capacities by changes in the unit-cell dimensions, channel, and cage sizes; 2) the transformation mechanics by the geometrical changes around the Ag1 linker and the bending and curving of the fluorous surface; 3) the sources of movement from the evolution of the multiple gas adsorption sites and their interactions with the skeleton. Why do FMOF-1 crystals show such a large, reversible, and anisotropic breathing induced by gaseous molecules? 1) The high flexibility of silver(I) coordination allows large framework expansion or contraction without any apparent bond breaking. 2) The fluorous surface has a low surface free energy and surface tension, which are known to stabilize surface bending or curving and are necessary to store a large amount of mechanical energy during reversible expansion and contraction processes. 3) The specific combination of the $(4^2.6)(4^4.6^2.8^8.10)$ gyroid topology and the interconnected channel voids surrounded by cages contributes to the large apparent PTE and NTE for the FMOF-1 crystal exposed to N_2 atmosphere, as predicted by Sigmund and Torquato.[23] Finally, we would like to point out that FMOFs have potential applications not only in gas storage and exchange but also in catalysis, sensing, and optoelectronic applications, such as n-type semiconductors for transistors and OLEDs.[24]

Received: September 28, 2008
Published online: January 9, 2009

Keywords: adsorption · crystal breathing · fluorinated ligands · metal–organic frameworks · thermal expansion

[1] G. Férey, *Chem. Soc. Rev.* **2008**, *37*, 191.
[2] a) O. M. Yaghi, M. O'Keeffe, N. W. Ockwig, H. K. Chae, M. Eddaoudi, J. Kim, *Nature* **2003**, *423*, 705; b) A. J. Fletcher, K. Thomas, M. Rosseinsky, *J. Solid State Chem.* **2005**, *178*, 2491.
[3] a) K. Uemura, R. Matsuda, S. Kitagawa, *J. Solid State Chem.* **2005**, *178*, 2420; b) S. Ma, D. Sun, X.-S. Wang, H.-C. Zhou, *Angew. Chem.* **2007**, *119*, 2510; *Angew. Chem. Int. Ed.* **2007**, *46*, 2458.
[4] a) C. Serre, C. Mellot-Draznieks, S. Surblé, N. Audebrand, Y. Filinchuk, G. Férey, *Science* **2007**, *315*, 1828; b) C. Serre, F. Millange, C. Thouvenot, M. Nogues, G. Marsolier, D. Louer, G. Férey, *J. Am. Chem. Soc.* **2002**, *124*, 13519.
[5] a) Y. Liu, J.-H. Her, A. Dailly, A. J. Ramirez-Cuesta, D. A. Brown, *J. Am. Chem. Soc.* **2008**, *130*, 11813; b) V. Finsy, H. Verelst, L. Alaerts, D. De Vos, P. A. Jacobs, G. V. Baron, J. F. Denayer, *J. Am. Chem. Soc.* **2008**, *130*, 7110; c) K. Kasai, M. Fujita, *Chem. Eur. J.* **2007**, *13*, 3089; d) S. Takamizawa, E. Nakata, T. Saito, *Angew. Chem.* **2004**, *116*, 1392; *Angew. Chem. Int. Ed.* **2004**, *43*, 1368.
[6] J. L. C. Rowsell, E. C. Spencer, J. Eckert, J. A. K. Howard, O. M. Yaghi, *Science* **2005**, *309*, 1350.
[7] J. L. C. Rowsell, J. Eckart, O. M. Yaghi, *J. Am. Chem. Soc.* **2005**, *127*, 14904.
[8] V. K. Peterson, Y. Liu, C. M. Brown, C. J. Kepert, *J. Am. Chem. Soc.* **2006**, *128*, 15578.
[9] C. Serre, S. Bourrelly, A. Vimont, N. A. Ramsahye, G. Maurin, P. L. Llewellyn, M. Daturi, Y. Filinchuk, O. Leynaud, P. Barnes, G. Férey, *Adv. Mater.* **2007**, *19*, 2246.

[10] a) C. Yang, X. Wang, M. A. Omary, *J. Am. Chem. Soc.* **2007**, *129*, 15454; highlighted in: R. A. Fischer, C. Wöll, *Angew. Chem.* **2008**, *120*, 8285; *Angew. Chem. Int. Ed.* **2008**, *47*, 8164; b) M. A. Omary, C. Yang, Patent Pending.
[11] I. J. A. Gladysz, D. P. Curran, I. T. Horváth, *Handbook of Fluorous Chemistry*, Wiley-VCH, Weinheim, **2004**.
[12] B. Ameduri, B. Boutevin, *Well-Architectured Fluoropolymers: Synthesis Properties and Applications*, Elsevier, London, **2004**.
[13] T. Nakajima, H. Groult, *Fluorinated Materials for Energy Conversion*, Elsevier, London, **2005**.
[14] A. L. Goodwin, M. Calleja, M. J. Conterio, M. T. Dove, J. S. O. Evans, D. A. Keen, L. Peters, M. G. Tucker, *Science* **2008**, *319*, 794.
[15] T. A. Mary, J. S. O. Evans, T. Vogt, A. W. Sleight, *Science* **1996**, *272*, 90.
[16] D. Dubbeldam, K. S. Walton, D. E. Ellis, R. Q. Snurr, *Angew. Chem.* **2007**, *119*, 4580; *Angew. Chem. Int. Ed.* **2007**, *46*, 4496.
[17] S. S. Han, W. A. Goddard III, *J. Phys. Chem. C* **2007**, *111*, 15185.
[18] R. Villalonga, R. Cao, A. Fragoso, *Chem. Rev.* **2007**, *107*, 3088.
[19] A. L. Spek, *J. Appl. Crystallogr.* **2003**, *36*, 7.
[20] A. Gupta, S. Chempath, M. J. Sanborn, L. A. Clark, R. Q. Snurr, *Mol. Simul.* **2003**, *29*, 29.
[21] F. Rouquerol, J. Rouquerol, K. Sing, *Adsorption by Powders & Porous Solids*, Academic Press, San Diego, **1998**.
[22] R. M. Prokop, A. W. Neumann, *Curr. Opin. Colloid Interface Sci.* **1996**, *1*, 677.
[23] O. Sigmund, S. Torquato, *Appl. Phys. Lett.* **1996**, *69*, 3203.
[24] S. M. Tekarli, T. R. Cundari, M. A. Omary, *J. Am. Chem. Soc.* **2008**, *130*, 1669.

